EJN
European Journal of Neuroscience

European Journal of Neuroscience, Vol. 28, pp. 1603–1616, 2008 doi:10.1111/j.1460-9568.2008.06477.x

NEUROSYSTEMS

Model of very fast (> 75 Hz) network oscillations generated by electrical coupling between the proximal axons of cerebellar Purkinje cells

Roger D. Traub,[1,*] Steven J. Middleton,[2,3] Thomas Knöpfel[3] and Miles A. Whittington[2]
[1]Departments of Physiology & Pharmacology, and Neurology, SUNY Downstate Medical Center, Brooklyn, NY, USA
[2]School of Neurology, Neurobiology & Psychiatry, The Medical School, Newcastle University, Newcastle, UK
[3]Laboratory of Neuronal Circuit Dynamics, RIKEN Brain Science Institute, Saitama, Japan

Keywords: cerebellar cortex, gap junction, network model

Abstract

Very fast oscillations (VFO; > 75 Hz) occur transiently *in vivo*, in the cerebellum of mice genetically modified to model Angelman syndrome, and in a mouse model of fetal alcohol syndrome. We recently reported VFO in slices of mouse cerebellar cortex (Crus I and II of ansiform and paramedian lobules), either in association with gamma oscillations (~40 Hz, evoked by nicotine) or in isolation [evoked by nicotine in combination with γ-aminobutyric acid $(GABA)_A$ receptor blockade]. The experimental data suggest a role for electrical coupling between Purkinje cells (blockade of VFO by drugs reducing gap junction conductance and spikelets in some Purkinje cells); and the data suggest the specific involvement of Purkinje cell axons (because of field oscillation maxima in the granular layer). We show here that a detailed network model (1000 multicompartment Purkinje cells) replicates the experimental data when gap junctions are located on the proximal axons of Purkinje cells, provided sufficient spontaneous firing is present. Unlike other VFO models, most somatic spikelets do not correspond to axonal spikes in the parent axon, but reflect spikes in electrically coupled axons. The model predicts gating of VFO frequency by g_{Na} inactivation, and experiments prolonging this inactivation time constant, with β-pompilidotoxin, are consistent with this prediction. The model also predicts that cerebellar VFO can be explained as an electrically coupled system of axons that are not intrinsic oscillators: the electrically uncoupled cells do not individually oscillate (in the model) and axonal firing rates are much lower in the uncoupled state than in the coupled state.

Introduction

We have described several types of fast oscillations (~30 Hz to over 150 Hz) that can be induced in somatosensory portions of mouse cerebellum *in vitro*, induced by activation of nicotinic receptors [sometimes with the added block of γ-aminobutyric acid $(GABA)_A$ receptors] or by low $[Ca^{2+}]$ media (Middleton *et al.*, 2008). The *in vitro* oscillations could be relevant to cerebellar fast oscillations *in vivo*, during putatively physiological states (Courtemanche & Lamarre, 2005) and pathological states (Cheron *et al.*, 2004, 2005a, b; Servais & Cheron, 2005; Servais *et al.*, 2005, 2007). All the cerebellar fast oscillations studied *in vitro* are suppressed by gap junction blockers (Middleton *et al.*, 2008); additionally, > 100 Hz cerebellar oscillations *in vivo* are also suppressed by carbenoxolone (Cheron *et al.*, 2005a, b; Servais *et al.*, 2005). Evidently, electrical coupling is critical for cerebellar fast oscillations, as it is for fast oscillations investigated in the hippocampus, entorhinal cortex (Draguhn *et al.*, 1998; Pais *et al.*, 2003; Cunningham *et al.*, 2004a, b; Nimmrich *et al.*, 2005; Roopun *et al.*, 2006). In the latter cortical fast oscillations, it is electrical coupling between principal neurons that appears to be critical, and a variety of data indicate that the most important site for this coupling lies on axons (Schmitz *et al.*, 2001; Traub *et al.*, 2003a, b; Roopun *et al.*, 2006; Hamzei-Sichani *et al.*, 2007).

Here, we focus on one particular type of *in vitro* cerebellar fast oscillation, that occurring at frequencies of ~100 to 150 Hz, in the presence of nicotine during blockade of $GABA_A$ receptors. We refer to it as cerebellar VFO (very fast oscillation). In addition to requiring electrical coupling via gap junctions, cerebellar VFO occurs independently of ionotropic glutamate receptors. Cerebellar VFO fields and optical signals have maximal amplitude in the granular layer, where the proximal unmyelinated axons of Purkinje cells lie; and cerebellar VFO is evident in Purkinje cell intracellular recordings (Middleton *et al.*, 2008), some of which show runs of spikelets (fast prepotentials).

The data suggest that cerebellar VFO might be induced by electrical coupling between Purkinje cell axons, in a manner analogous to that proposed for 200-Hz ripples induced in hippocampal slices by low-$[Ca^{2+}]$ media (Draguhn *et al.*, 1998; Traub *et al.*, 1999; reviewed in

Correspondence: Dr R. D. Traub, *present address below.
E-mail: rtraub@us.ibm.com

**Present address*: IBM T.J. Watson Research Center, Yorktown Heights, NY 10598, USA.

Received 10 June 2008, revised 23 August 2008, accepted 28 August 2008

Traub *et al.*, 2002). The latter model was based on several assumptions: (i) principal cell axons were electrically coupled to one another in a sparse network; (ii) the gap junctions allowed an action potential in one axon to induce an action potential in a coupled axon, after a brief latency; (iii) axons had strong but brief refractoriness; (iv) there was a background of rare spontaneous action potentials. A 'percolation' model like this could generate VFO, with spikelets (Traub *et al.*, 1999).

Here, we describe a network model of cerebellar VFO, using 1000 multicompartment Purkinje cells, coupled via gap junctions on their proximal axons. This model generates field oscillations and intracellular potentials resembling experimental data. The physical principles are, however, somewhat different than in the percolation model.

Materials and methods

In vitro mouse cerebellar slice experiments

Slice preparation

Coronal sections, 400 μm thick, of cerebellum containing Crus 1 and 2 of the ansiform and paramedian lobules, were prepared from adult male C57b6 mice. Animals were administered terminal anesthesia with isoflurane and ketamine/xylazine, and then perfused with sucrose solution. All procedures conformed to the UK Home Office Animals (Scientific Procedures) Act 1986. Slices were maintained at the interface between artificial cerebrospinal fluid (aCSF) containing (in mM): NaCl, 126; KCl, 3; NaH_2PO_4, 1.25; $CaCl_2$, 2; $MgSO_4$, 1; $NaHCO_3$, 24; glucose, 10; and warmed, wetted 95% O_2/5% CO_2 at 35 °C. The rhythmogenic compound nicotine (10 μM) was bath applied with gabazine (2 μM) to generate a VFO. β-Pompilidotoxin (10 μM) was subsequently applied following stabilization of VFO area power (80–400 Hz). All drugs were obtained from Tocris (UK).

Electrophysiology

Field potential recordings were obtained from the Purkinje cell layer using glass micropipettes (0.5–2 MΩ) filled with aCSF. Data were broadband filtered at 1 Hz–20 kHz to assess both local field potential and multiunit activity. Multiunit activity was found to be highly locally synchronous, generating population spiking that was evident with more narrow low-pass filtering below 400 Hz. To optimize signal/noise ratios, data are therefore presented band-pass filtered in the range 1–400 Hz. Intracellular recordings (0–10 kHz) from Purkinje cells were obtained using glass pipettes (50–90 MΩ) filled with 2 M potassium methylsulfate. Power spectra were constructed using AXOGRAPH software and statistical analysis performed using paired *t*-tests, with significance set at $P < 0.05$.

Purkinje cell spikelet homogeneity was quantified in somatic sharp electrode recordings, using the spike sorting tool 'Wave_clus' (Quian Quiroga *et al.*, 2004). Thresholds were set to exclude all full action potentials, but to include > 95% of spikelets detectable 'by eye'. Spikelets were identified automatically by a series of wavelet coefficients that best described the spikelet shape. Wavelet coefficients were fed into a clustering algorithm to quantify automatically the degree of similarity of spikelet shapes across the entire detected spikelet population – with the most similar spikelet shapes automatically grouped together into separate populations (clusters). Parameters for this automatic clustering algorithm were set to optimize the ability to detect different populations of spikelets if present: minimum cluster size was set to 2% of total spikelets detected. Temperature, as an equivalent of spikelet covariance (affecting the likelihood of any set of different spikelets being assigned to the same cluster), was set to give at least two clusters in each dataset. From this, homogeneity was quantified as the proportion of spikelets in the largest cluster with respect to total spikelets detected. In other words: what proportion of the total spikelet shapes detected was statistically 'the same'? This method was also applied to simulation data.

Simulations

The building block of the network simulations was a 559-compartment model of a single Purkinje cell (see Appendix). This model had a six-compartment 60-μm segment of unmyelinated axon, a soma, dendritic shaft, and smooth and spiny dendritic regions. [This axon is somewhat longer than reported for the rat Purkinje cell axon initial segment (Clark *et al.*, 2005), but the gap junctions are restricted (see below) to the proximal 30 μm. The axon was extended a bit for the sake of numerical stability.] The model contained 12 active conductances, including fast (transient) and persistent g_{Na}, six types of g_K, three types of g_{Ca} and an anomalous rectifier. This model included a full range of conductances, so that it would be available for a variety of applications. In the present simulations (except in the Appendix), however, Ca^{2+} and Ca^{2+}-dependent conductances were shut off, as were the anomalous rectifier and the 'D' type of slowly inactivating K^+ current; this was done for the sake of simplification. (Removing Ca^{2+} and Ca^{2+}-dependent conductances is reasonable as a first approximation, as cerebellar VFO can occur in low [Ca^{2+}] media.)

For network simulations, we took 1000 copies of the single Purkinje cell model, and introduced gap junctions between pairs of cells, randomly assigned (Erdös & Rényi, 1960) at pre-selected compartments on the model neurons. To construct the network, the total number of gap junctions to be used was first set, as a parameter; and allowable compartments for gap junctions were specified. Pseudo-random pairs of cells were then chosen, one by one, as well as pseudo-random choices for the sites of each gap junction on each cell: these data were stored in a table (we call the choices 'pseudo-random' because a pseudo-random number generator is used by the program). There were no chemical synapses. In preliminary simulations, gap junctions could occur between dendritic sites, between somata or between axons, in various combinations. We found that gap junctions between somatic and dendritic sites did not contribute to collective population oscillations (because coupling potentials were so small), and therefore the data we describe here derive only from simulations in which gap junctions were restricted to axons. For the data to be illustrated, we used simulations in which gap junctions were restricted to the proximal three axonal compartments (30 μm of unmyelinated axon), at a density of 5 gap junctions lying on each axon (on average), and with gap junction conductance = 6 nS. [If the gap junctions were to contain connexin36 (Hamzei-Sichani *et al.*, 2007), with unitary conductance of about 10–15 pS (Srinivas *et al.*, 1999), this parameter choice corresponds to using 400–600 connexons per gap junction; 400–600 connexons is a plausible estimate, because Hamzei-Sichani *et al.* found about 100 connexons in a single small gap junction plaque, and found that five small plaques could be arranged in a row with mean spacing of 115 nm.] With a gap junction conductance of 6 nS, we never observed a case where a single axonal spike in one axon would induce a spike in an electrically coupled axon, even when gap junctions were located in the most distal axonal compartment; for this reason, the present network model can not exhibit percolation (Traub *et al.*, 1999), and alternative VFO mechanisms needed to be sought. It is, of course, conceivable that a single axonal spike might induce an axonal spike in a coupled neuron, in a case where electrical coupling occurs between nodes of Ranvier (Yasargil & Sandri, 1987), but this possibility was not investigated in the present model.

The random gap junctional connectivity introduces heterogeneity into the system, but additional heterogeneity was added by using

randomly distributed somatic bias currents of 0.35–0.45 nA. A few of the neurons had somatic hyperpolarizations of −0.25 nA, to lower full-spike firing rates and to help unmask spikelets (although spikelets occurred as well in cells that were not hyperpolarized); spikelets in turn could be compared with experimental spikelets and were an indicator of axonal firing. Axons were slightly depolarized (0.04 nA to each axonal compartment) in order to raise their excitability and spontaneous activity, as is likely to occur in nicotine (Kawai *et al.*, 2007) or in low-calcium media.

An additional source of heterogeneity occurred in the form of ectopic axonal spikes, generated by a Poisson process that injected current pulses (0.45 nA, 0.8 ms) into the distal axon, at mean rates of 13.33–40 Hz/axon. Again, the ectopic spikes are presumed to reflect increased axonal excitability caused by nicotine (Kawai *et al.*, 2007) or low-calcium media – although a direct origin of ectopic spikes in axons remains to be shown experimentally. In previous models of axonal plexus VFO (e.g. Traub *et al.*, 1999), it was possible to use ectopic rates as low as 0.05 Hz/axon, but that was in cases in which action potentials could propagate directly from axon to axon. In the present model, such propagation does not occur (i.e. a spike in a single axon would not induce a spike in a single coupled axon), so that much higher spontaneous activity rates were necessary for population oscillations to occur.

The 'field' produced by a given simulation was estimated, either by averaging all of the somatic potentials or all of the potentials at a fixed mid-axonal site; these averages were then inverted, so as to resemble the experimentally recorded fields. Somatic and axonal 'fields' had similar shapes, with the axonal 'field' shifted about 5 mV, reflecting a net mean depolarization of axons relative to somata.

Code was written in Fortran, augmented with mpi to run in a parallel environment, using a variation of the code reported in Traub *et al.* (2005). Programs were run on 50 central processing units (cpus) of an IBM 1350 Linux cluster. A 175-ms simulation lasted about 21.5 h.

Copies of the original code can be obtained by writing to roger.traub@downstate.edu or rtraub@us.ibm.com. In addition, source Fortran code (for a single Purkinje cell and for the 1000-cell network) is available at the ModelDB website at Yale University, http://senselab.med.yale.edu/modeldb/ShowModel.asp?model=114654.

Results

The network model generates very fast network oscillations when axons are electrically coupled

We first note that experimental field potential recordings from mouse cerebellar slices, bathed in nicotine to induce gamma oscillations (∼40 Hz), will subsequently generate VFO upon further blockade of $GABA_A$ receptors with gabazine (∼100 Hz; Middleton *et al.*, 2008). Data such as these, together with the insensitivity of experimental cerebellar VFO to blockade of α-amino-3-hydroxy-5-methyl-4-isoxazolepropionic acid (AMPA), *N*-methyl-D-aspartate (NMDA) and $GABA_B$ receptors, and the sensitivity to carbenoxolone and other gap junction blockers (Middleton *et al.*, 2008), all render plausible our assumption that it is solely electrical coupling that brings about the very fast network oscillation. In accord with this notion, Fig. 1 illustrates an example of network oscillations produced by the 1000-cell Purkinje cell model, with gap junctions between proximal axonal sites (five per axon on average, conductance 6 nS, ectopic rate = 13.3 Hz on average per axon). Oscillation amplitude decreased, or the oscillation would slow or even disappear, on using: (i) fewer axonal coupling sites (with no oscillation at all when using 2.5 gap junctions per axon on average, and only an initial and transient oscillation, < 100 ms, with 4 gap junctions per axon – the transience resulting because the neurons begin somewhat more depolarized than in the steady-state, as the bias currents come into play); (ii) a smaller gap junction conductance (frequency 80 Hz with 5.5 nS conductance, and no oscillation with 5.0 nS conductance) and lower ectopic rates (so that, e.g. ectopics at 4 Hz produced a slowing attenuating oscillation over ∼100 ms that then disappeared – again, the transience occurred because of an initial relative depolarization). As will be seen below, increasing the ectopic spike rate increased the population frequency. The detailed mechanisms by which the network oscillation is actually generated will be clarified in subsequent figures.

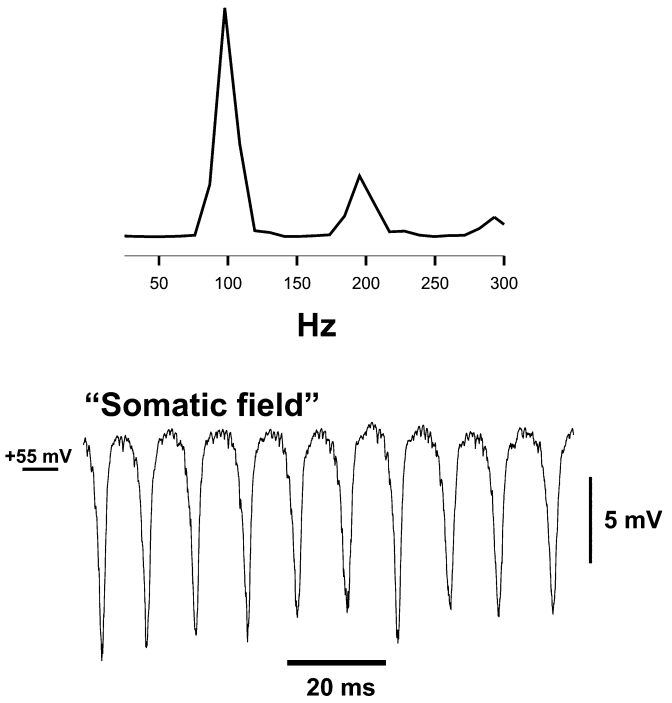

FIG. 1. VFO in network model. Data from a simulation with 1000 model Purkinje neurons, with gap junctions located on the proximal axons, average 5 gap junctions per cell. The power spectrum (peak at ∼100 Hz) is shown above; the 'field' consists of the inverted average of all somatic potentials in the population. (The 'axonal field', not shown, has a similar shape to the somatic field, but is shifted ∼5 mV, reflecting a relative mean depolarization of the axons.) For comparable experimental field data, in nicotine + gabazine, see Middleton *et al.* (2008).

The network model generates barrages of variable amplitude spikelets, as can be observed experimentally

Figure 2A demonstrates an example of the variable-amplitude spikelets that can occur in Purkinje cells during VFO induced by nicotine and gabazine (spikelets of similar appearance have also been recorded in cerebellar Purkinje cells *in vivo*; S. J. Middleton and T. Knöpfel, unpublished data); the figure shows as well the appearance of similar potentials in a model Purkinje cell (hyperpolarized with −0.25 nA somatic current injection, to partially suppress full somatic spikes) during the simulated network oscillation. Of special note are the spikelets (*) that occasionally occur just prior to a full action potential, both in experiment and model. Patterns of polymorphic spikelets, similar to those in the 'model' part of Fig. 2A, were observed in all seven of the other hyperpolarized Purkinje cells from this simulation. Spikelets also occurred in model Purkinje cells that

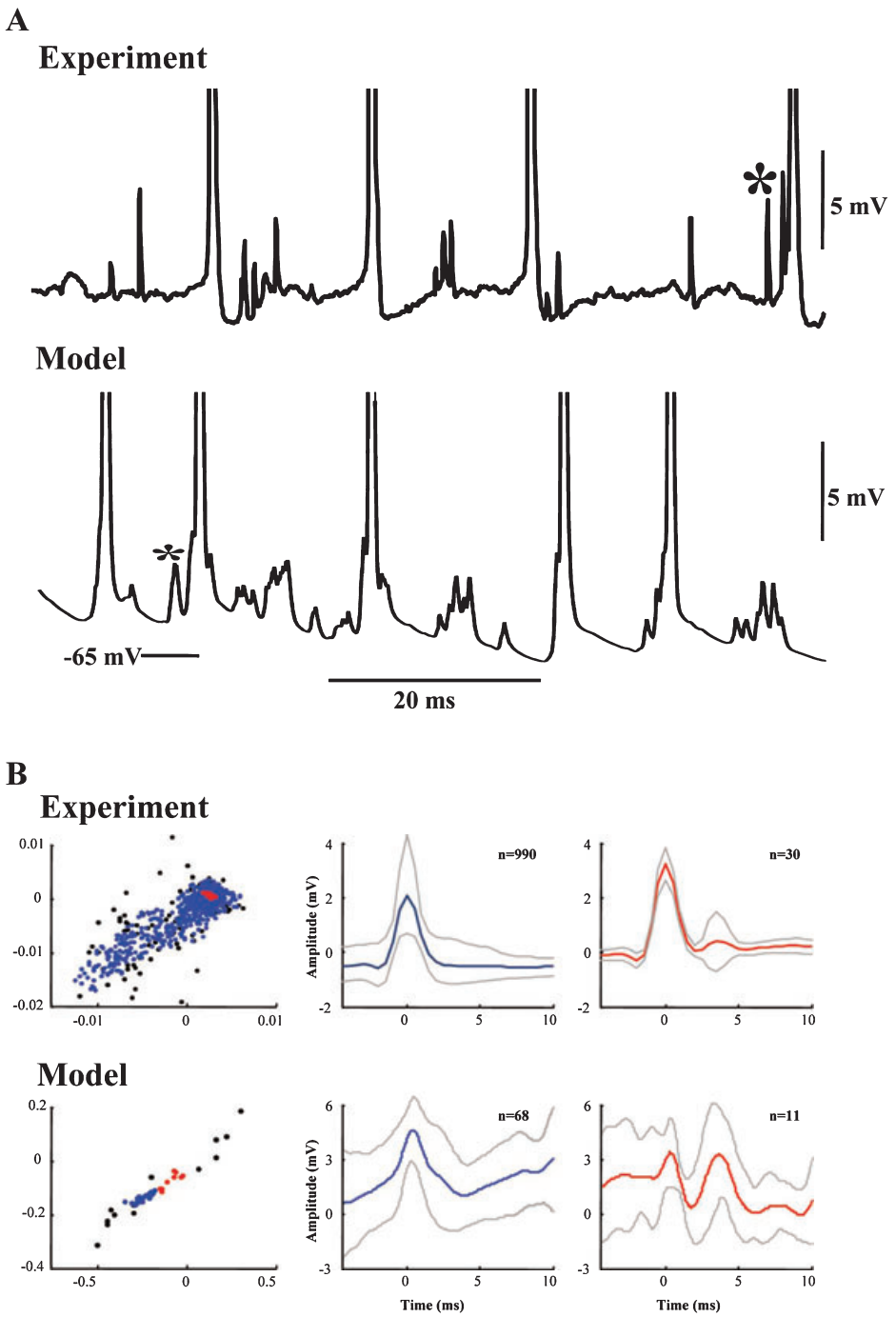

FIG. 2. VFO-associated spikelets in a mouse Purkinje cell and a model Purkinje cell. (A) In some Purkinje cells, barrages of spikelets occur at varying amplitudes (Middleton *et al.*, 2008) and similar barrages occur in the somata of Purkinje cells during network VFO in the model. On occasion (*), spikelets occur just prior to full action potentials (which are truncated in both experimental and model records). (B) Results from cluster analysis of spikelets recorded from Purkinje cell somata (experiment) or present in somatic compartments in the Purkinje cell network model. Experimental data (upper panels) were taken from a set of 1080 spikelets. Left graph shows the distribution of spikelet properties as first vs. second wavelet coefficients. Spikelets in the largest cluster (blue) show large, approximately linear variability in wavelet coefficients. Spikelets in the second largest cluster are shown as red symbols, and all remaining spikelets are shown as black symbols. Middle and right graphs show the mean (± SD) spikelet shapes for the largest and second largest clusters, respectively. Ninety percent of spikelets form the large cluster. The lower panel shows the results from the same cluster analysis applied to model data containing 91 spikelets. The distribution of spikelet properties showed a similar coefficient variability to the experimental data. Seventy-five percent of spikelets form the large cluster. Note that, both in experiment and model, the spikelets in the second largest cluster did not appear to have different shapes compared with those mapped to the largest cluster, but rather were occurring in multiplets rather than singlets.

were not hyperpolarized, although admixed with more full action potentials (not shown).

Spikelets of somewhat similar appearance to Fig. 2A (*) are also noted in layer 5 intrinsically bursting pyramidal cells in somatosensory neocortex, during the beta2 (~25 Hz) oscillation induced in somatosensory cortex slices by kainate – another network phenomenon attributable to gap junctional coupling (Roopun *et al.*, 2006). In general, however, spikelets in layer 5 pyramidal cells are not

polymorphic in the way Purkinje cell spikelets were. There are two possibilities that might explain variation in shape and amplitude of the spikelets: first, there might be coupling between different regions of the cells, e.g. axons, somata and dendrites; second, the coupling might all lie between homologous regions (e.g. all between axons, as used in the model described here), but at different electrotonic distances from the soma. In the first case, one might expect utterly distinct categories of spikelet shapes, as illustrated for dendritic vs. axonal electrical coupling between pyramidal cells (see fig. 4 of Draguhn *et al.*, 1998). In the second case, one would expect a continuous smooth distribution of spikelet shapes and amplitudes. We addressed this quantitatively by using an unsupervised spike-sorting algorithm (Quian Quiroga *et al.*, 2004) applied to spikelets (see Materials and methods). The results, shown in Fig. 2B, demonstrate that the overwhelming majority of spikelets (both experimental and simulated) lie in a single, statistically significant cluster, characterized by a continuous distribution of wavelet parameters that define spikelet shape. Most of the spikelets lying outside this main cluster (again, both in experiment and model) were multiplets, unlike the singlet spikelets in the main cluster. Thus, the results in Fig. 2B were consistent with the second of the above described possibilities: that spikelets arise from electrical coupling between homologous cell regions, with differences in electrotonic distance from the soma. The model indicates that the cell region involved is the axon. [Note the smaller number of data points for the model as compared with experiment: this was necessitated by the very long computation times for the simulations (Materials and methods).]

Spikelets in the network model usually result from full action potentials in coupled axons, but not from full action potentials in the parent axon

In previous models of gap junction-mediated network oscillations (e.g. Traub *et al.*, 1999, 2005; Cunningham *et al.*, 2004a; Roopun *et al.*, 2006), principal cell spikelets were uniformly induced by full action potentials in the parent axon of the respective principal neuron in whose soma the spikelet was observed. These cells, therefore, appear to express 'partial' spikes as classically described in spinal motor-neurons (Coombs *et al.*, 1957). In contrast, in Purkinje cells axonal action potentials reliably invade the soma to trigger full action potentials, according to Clark *et al.* (2005) and Khaliq & Raman (2006). Therefore, we are not surprised that, in the present model, as Fig. 3 makes clear, somatic spikelets were not induced by action potentials in the parent axon. As Fig. 3A2 shows, somatic spikelets corresponded instead to slightly larger spikelets in the parent axon, and not to full spikes in the parent axon; when the parent axon fired a full spike, so did the soma. On the other hand, spikelets in the parent axon (and soma) corresponded to full action potentials in electrically coupled axons (compare Fig. 3A1 with Fig. 3B, the respective

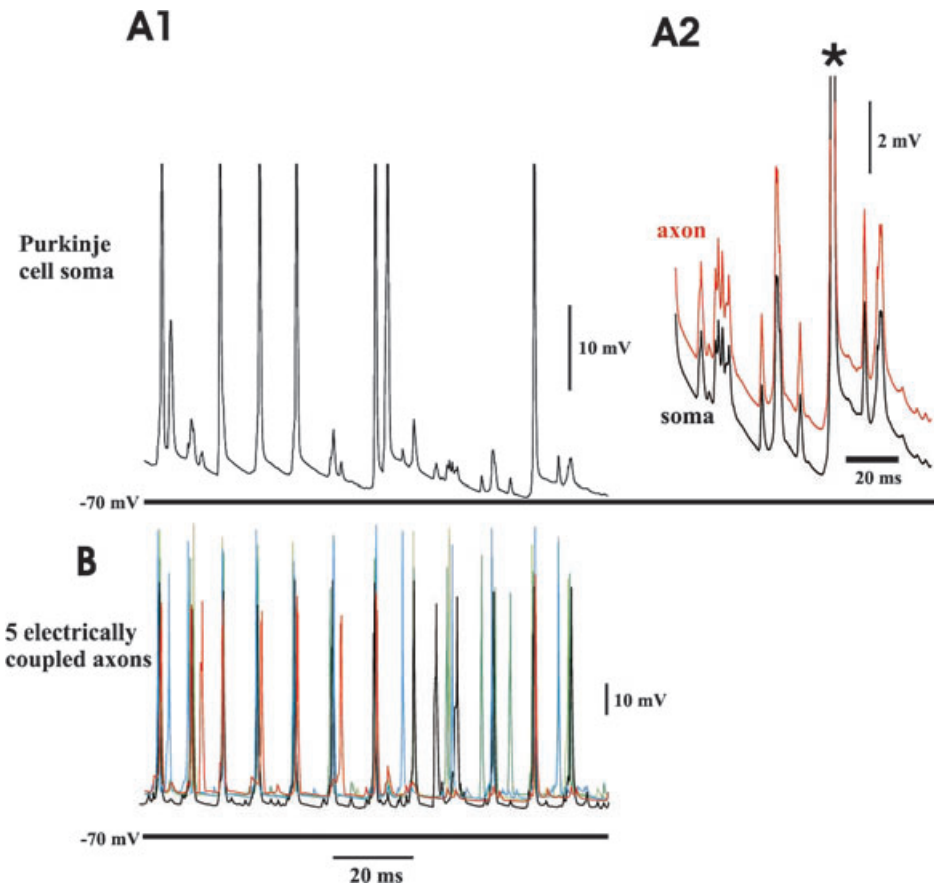

FIG. 3. In the network model, somatic spikelets do not (in general) correspond to full action potentials in the parent axon, but do correspond to full action potentials in one or more electrically coupled axons. (A1) Somatic trace of a hyperpolarized Purkinje cell, showing multiple spikelets of variable amplitude. (A2) Expansion of part of the trace in (A1) (around the last somatic action potential, *), also showing the simultaneous voltage at an axonal site. There is a one-one correspondence of somatic spikelets with axonal spikelets. (B) Five axons that are electrically coupled to the cell shown in (A), in a trace that is concurrent with the somatic trace of (A1). Every somatic spikelet (and also full action potential) is tightly correlated with a full spike in one or more of the coupled axons. (Data from the same simulation as Fig. 2.)

potentials being 'recorded' simultaneously – Fig. 3B shows all of the axons to which the parent axon was coupled).

Thus, the somatic spikelets in our Purkinje cell network model resemble conventional electrical coupling potentials, more than they resemble the axonal coupling situation described previously (e.g. Traub *et al.*, 1999; Schmitz *et al.*, 2001); in this previous situation, a spike in one axon induces (in the model), or is presumed to induce (in the experiments), a full spike in a coupled axon that then propagates antidromically to the soma and, if this propagation is decremental, the antidromic propagation results in a somatic spikelet.

If, then, the gap junctions in our present model are simply inducing conventional coupling potentials, does that imply that the model consists simply of a set of Purkinje cell intrinsic oscillators that are synchronized by the gap junctions? The answer is definitively 'no', as the next figure demonstrates.

Electrical coupling in the network model increases axonal firing rates, as well as providing temporal organization of the activity

Our Purkinje cell network model is not behaving as a system of coupled oscillators in two fundamental respects, both clear in Fig. 4: (i) the uncoupled neurons are not regular oscillators, but rather their axons are induced to fire by independent Poisson processes (see also Materials and methods); (ii) there are more than three times as many axonal spikes per unit time in the coupled network compared with the uncoupled network [see also the network behavior in Roopun *et al.* (2006) – both experimental and simulated – in which firing rates are higher in the coupled systems than in the uncoupled systems; see, as well, Maex & De Schutter (2007), who also observed an increase of firing rates with weak coupling]. Evidently, our Purkinje cell network model is producing collective oscillations as an emergent process, with the gap junctional coupling increasing the firing probability of each given axon, as well as providing temporal organization to the population as a whole. How can this be, given that one does not see axonal spiking in one cell induce axonal spiking in a coupled cell (Fig. 3)? Our presumption is that the occurrence (within a narrow time window) of axonal spikes in n or more cells ($n > 1$) – all of these axons being coupled to an observed axon – will suffice to induce a spike in the observed axon. This notion (that two or more coincident axonal spikes can induce a spike in a coupled axon) would be in accord with the requirement, in the model, for a high rate of spontaneous firing, as well as for a high density of gap junctions (five per neuron, far above the so-called percolation limit of 1 gap junction per axon; Erdös & Rényi, 1960). In contrast, previous models of axonal plexus VFO, in which single spikes could cross from one axon directly to another axon, could work with very low ectopic rates (< 0.1 Hz vs. > 13 Hz used here) and very sparse gap junctional coupling (e.g. 1.6 gap junctions per axon, on average, vs. the 5 gap junctions on average used here; Traub *et al.*, 1999).

We tested the hypothesis that multiple axonal spikes in coupled cells were required to induce an axonal spike in another cell, as follows. We repeated the simulation used in Figs 3 and 4 twice, concentrating on a particular Purkinje cell (#21) over a few-ms interval during which its axon fires (Fig. 5). First, we plot the action potentials of the five axons electrically coupled to cell #21, starting at time 77.5 ms (Fig. 5A – here, 'control' refers to the simulation used in Figs 3 and 4). Figure 5B, 'control', shows the corresponding voltage for the axon of cell #21 itself (black trace). Next, we repeated the entire simulation, but starting at time 77.5 ms we unidirectionally blocked the gap junction between axon #168 and axon #21: axon #168 was the first coupled axon to fire in Fig. 5A, and we prevented current

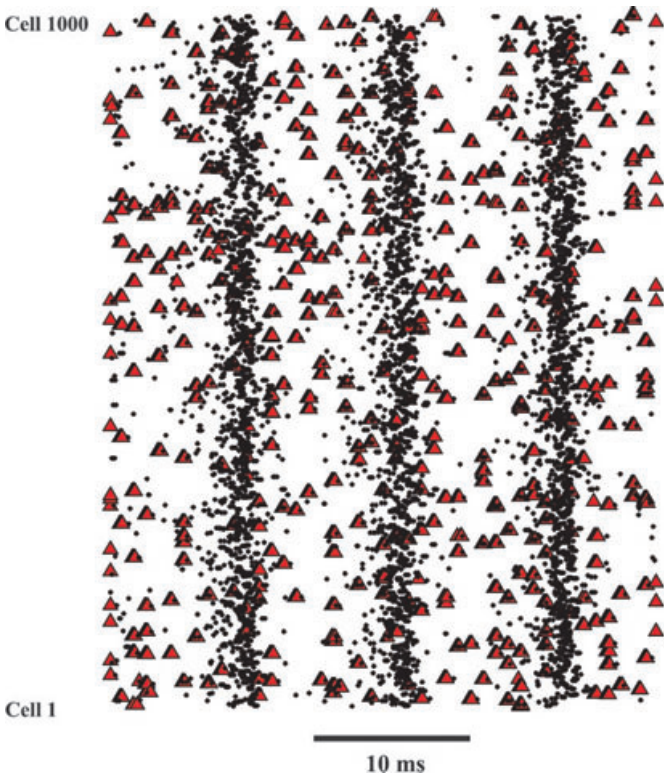

FIG. 4. Gap junctions increase axonal firing, in addition to producing oscillatory (rhythmic) temporal organization. Raster plots were constructed by probing the mid-axonal (third compartment from the soma) potential of each model Purkinje cell, every 0.045 ms, and writing into a file the time and cell number if this potential was > 0 mV, i.e. overshooting. (This procedure on occasion counts a single axon potential or tight doublet twice, so it is not perfectly precise to say that it counts 'spikes'.) Red triangles indicate overshooting times when the axons are all electrically uncoupled, but subject to Poisson-distributed depolarizing pulses (0.45 nA, 0.8 ms, to one axonal compartment) at a mean rate of 13.3 Hz/axon. There are 5879 'overshooting events' per 100 ms, scattered irregularly (so that somewhat under 50% of the depolarizing pulses actually leads to an axonal action potential). In contrast, black dots are axonal overshooting events from a simulation with identical parameters – including the axonal depolarizing pulses, which are given at exactly the same times – but with electrical coupling between the axons (6 nS coupling conductance, average of 5 gap junctions per axon, gap junctions on three most proximal axonal compartments). In this case, there are 19 999 'overshooting events' per 100 ms (i.e. a 3.4-fold increase in axonal activity), now organized into a population oscillation.

from flowing from this axon to axon #21. This manipulation delays the firing of axon 21 by about 1 ms (Fig. 5B, green trace). Finally, we prevented current flow from two early-firing coupled axons to axon #21. In this case, axon #21 did not fire at all (Fig. 5B, red trace), even though two other coupled axons (#28 and #304) fire at nearly the same time as the blocked axons (axon #99 required input from axon #21, and so did not fire during the 'red' simulation, but axons #28 and #304 did actually fire – not shown). Thus, at least in this instance, multiple near-simultaneous firings of couple axons seem to be required to induce firing in a given axon.

What determines the period of the network oscillation? In previous axonal plexus VFO models (e.g. Traub *et al.*, 1999; Lewis & Rinzel, 2000), wherein a single axonal spike could induce a spike in a coupled axon, a major determinant of the oscillation period was the gap junctional connectivity; and the intrinsic properties of the axons played virtually no role in determining the population period. It was possible to manipulate the connectivity over a range of ~1.5 gap

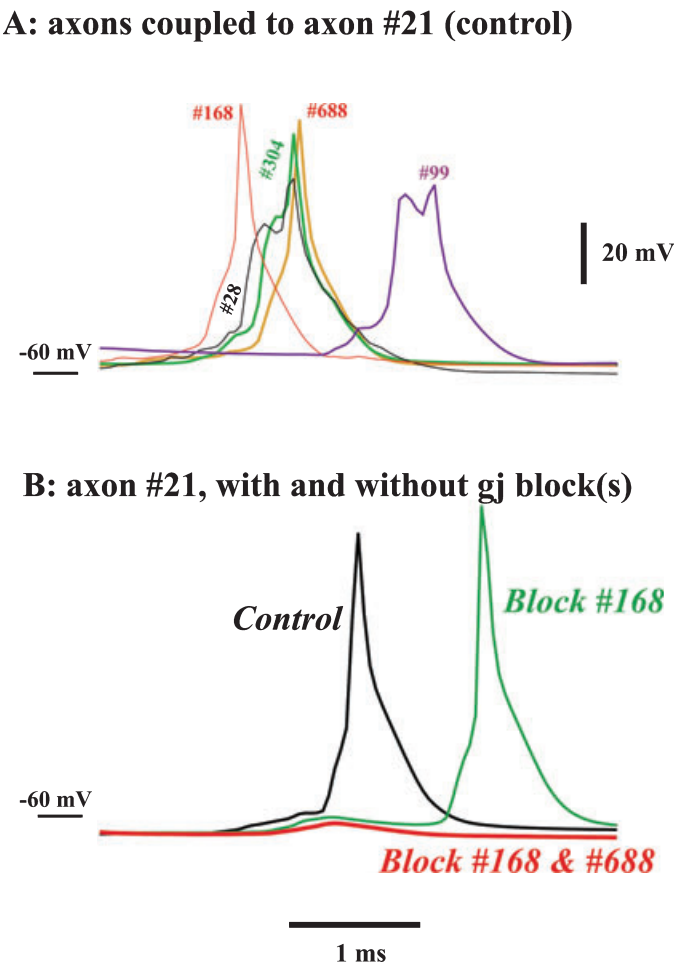

FIG. 5. Multiple axonal spikes are required to induce an axonal spike in a coupled cell. (A) The potentials of five axons that are electrically coupled to the axon of Purkinje cell #21, starting at time = 77.5 ms, in the simulation used for Figs 3 and 4. The axons are labeled and plotted in different colors. (B) The potential in the axon of cell #21, also starting at time = 77.5 ms, in control conditions [black, same simulation as in (A)]; in conditions where axon #168 ceases to influence axon #21 at time = 77.5 ms (green – note the delay in the spike in axon #21); and in conditions where both axons #168 and #688 cease to influence axon #21, starting at time = 77.5 ms (red – note the suppression of firing in axon #21, despite firing in axons #28 and 304).

junctions per axon (on average) to over 3. In contrast, in the present model, there is an absolute requirement for high gap junctional connectivity, which makes it likely that some other parameter(s) determined the period. In another model of Purkinje cell axonal plexus oscillations (Maex & De Schutter, 2007), axon/soma conduction times contributed significantly to the period; that model, however, used a very long unmyelinated axon, up to 1 mm. Our model, in contrast, uses a rather short unmyelinated axon (Eccles *et al.*, 1967; Palay & Chan-Palay, 1974; Kato & Hirano, 1985), and axon/somatic conduction times are very short (Fig. 3A2). We therefore asked whether intrinsic membrane conductance kinetics might be determining the oscillation period, in the present model, and in contrast to previously investigated percolation-type VFO models (Traub *et al.*, 1999). As it is the axons that initiate the firing, we concentrated on membrane kinetics there. We noted (not shown) that blocking the persistent Na^+ conductance had only a small effect on the network oscillation, and so therefore concentrated on the axonal transient Na^+ conductance and on axon K^+ conductances.

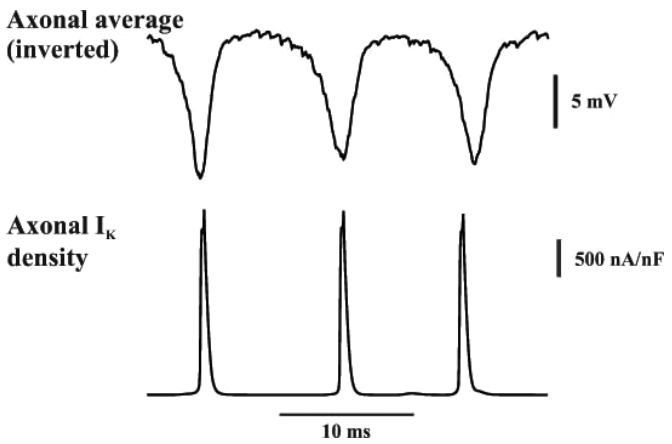

FIG. 6. Period of simulated network VFO is not gated by axonal K^+ conductances. Plotted are the axonal 'field' (i.e. the inverted average axonal potential at one site in the distal axons), and axonal I_K density in an adjacent axonal compartment of a single neuron. This current density falls to virtually zero between field minima.

Oscillation period in the network model is not gated by axonal K^+ currents

As Fig. 6 makes clear, axonal K^+ currents are phase-locked to the population oscillation – hardly surprisingly – but the current between axonal population spikes falls to virtually zero. This makes it unlikely that the oscillation period is determined by such currents, at least in a direct fashion. [There are, however, indirect effects (not shown), as K^+ currents will influence action potential amplitude and width, and hence the manner in which one axon influences a coupled axon. For example, if delayed rectifier g_K density was increased by 50%, the oscillation was blocked; and if it was decreased by 30%, the oscillation became faster and of higher power (by indirectly strengthening the effective coupling between axons).]

Oscillation period in the network model is determined by recovery from transient Na^+ current inactivation

The kinetics of the transient Na^+ conductance inactivation (Hodgkin-Huxley '*h*', see Materials and methods) were directly coupled to the field oscillation in our model (Fig. 7A). (In this simulation, the ectopic spike rate was, on average, 40 Hz per axon, so that the baseline population frequency here is faster than for previous simulations.) Furthermore, when inactivation kinetics in the network model were slowed by 50%, the network oscillation slowed from 141 to 98 Hz (Fig. 7B); and when inactivation kinetics were sped up by 50%, the oscillation frequency increased to 152 Hz (not shown). Note that activation kinetics of the transient Na^+ conductance are much faster than the oscillation period, and can not directly gate the period. A corresponding reduction of oscillation frequency also occurred when transient Na^+ conductance inactivation kinetics were slowed by 50%, using the original ectopic spike rate of 13.3 Hz per axon: from 98 to 76 Hz (not shown).

The conceptual scheme for the network oscillation, suggested by the simulations, would then be as follows: suppose the Purkinje cell axons all fire together on a particular VFO wave, and their Na^+ conductances inactivate roughly in phase. As recovery from inactivation proceeds, noise (in the form of ectopic axonal spikes) occurs and eventually several axons begin to fire. If there is enough noise, and if axonal refractoriness has recovered enough, there will be instances of

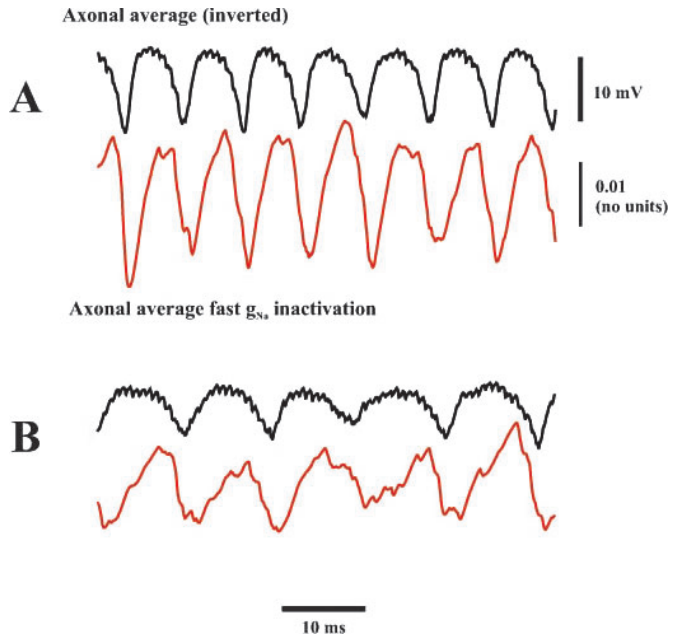

FIG. 7. Period of simulated network VFO is gated by the kinetics of transient g_{Na} inactivation (Hodgkin–Huxley '*h*' variable). (A) Baseline simulation, showing (black) the axonal 'field' (as in Fig. 6) and the average value (averaged across the population of 1000 model Purkinje cells, red) of '*h*' for transient g_{Na}, at a mid-axonal compartment. Same simulation as in previous figures, except for a higher axonal noise rate (40 Hz). The population oscillation frequency is 141 Hz. (B) The simulation of (A) was repeated, but with the kinetics of '*h*' for transient g_{Na} at half the usual value (i.e. the Hodgkin–Huxley rate functions α_h and β_h were each multiplied by 0.5). The population frequency is now 98 Hz.

multiple firings in axons that are all coupled to the same axon, and propagation can then provide amplification in the degree of firing, above and beyond what occurs from the ectopic process by itself. This amplification in turn eventually leads to the next VFO wave (Fig. 4). This scheme is consistent with the period-dependence on Na^+ conductance kinetics, as well as on the need for large numbers of gap junctions and high ectopic rates. The scheme is roughly analogous to the growth process that leads to an action potential in a single axon, with the following set of equivalences:

1) single axon individual Na^+ channel – an axon in the population
2) opening of the individual Na^+ channel – a spike in one axon
3) stochastic single-channel openings – ectopic spikes in the network
4) current flowing through an open channel depolarizing the membrane and tending to open other channels – current from a spike in one axon depolarizing other axons through gap junctions.

Our previous models of VFO (e.g. Traub *et al.*, 1999) would then be analogous to a situation where stochastic opening of a single Na^+ channel could lead to a full action potential, assuming the membrane to be at rest; whereas the present Purkinje cell network model is analogous to the (more usual) case where a number of Na^+ channels must open for a spike to occur, even with the membrane at rest or nearly so. Furthermore, in our previous VFO model (Traub *et al.*, 1999), intrinsic membrane properties did not significantly influence the population period, whereas in the present VFO model intrinsic membrane properties clearly do influence the period.

Experimental evidence, using β-pompilidotoxin, that cerebellar VFO period is also gated by transient Na^+ current inactivation

The wasp venom toxin β-pompilidotoxin has been reported to slow the kinetics of Na^+ channel inactivation (Grieco & Raman, 2004). We therefore were able to test the prediction of Fig. 7 experimentally (Fig. 8). (The experiment was done after the simulations.) Network oscillations were induced in mouse cerebellar slices with nicotine (10 μM) and gabazine (2 μM), as described elsewhere (Middleton *et al.*, 2008). Mean peak frequency of the very fast network oscillation was 139 ± 3 Hz before application of the toxin, while following β-pompilidotoxin application (10 μM), the mean peak frequency shifted to 98 ± 4 Hz. (This change was significant, $P < 0.01$, paired *t*-test, $n = 5$.) Thus, this experiment was indeed consistent with the model prediction.

Discussion

In this paper, we have proposed a network model of cerebellar VFO that is based primarily on *in vitro* data (Middleton, 2005; Middleton *et al.*,

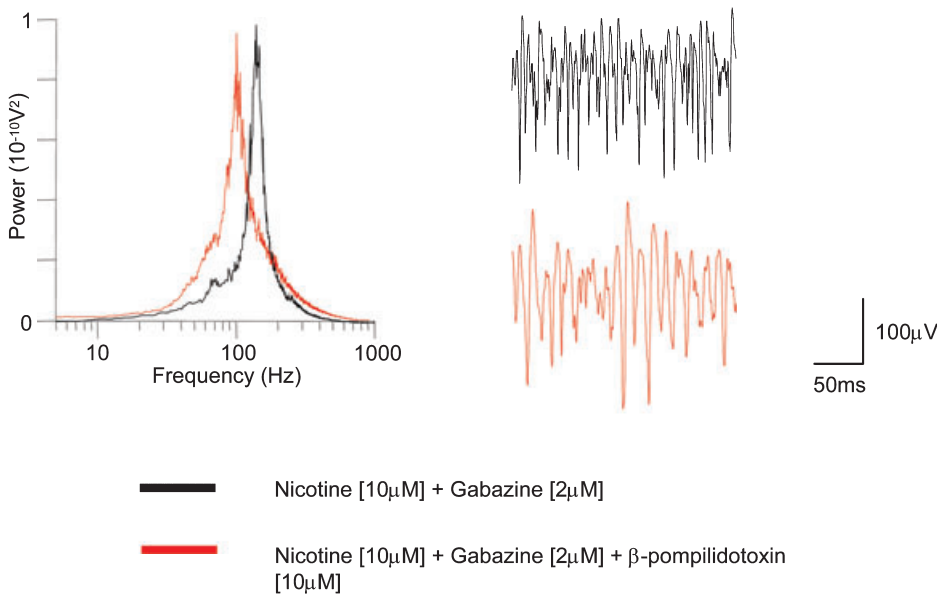

FIG. 8. Experimental evidence (using β-pompilidotoxin) that cerebellar network VFO are also gated by the kinetics of transient g_{Na} inactivation. See text for details.

2008). The model consists of 1000 Purkinje cells, electrically coupled via their proximal axons, with an average of 5 gap junctions lying on each axon; there are no chemical synapses in our model. This model generates VFO under conditions of high spontaneous rates of axonal spiking activity – simulated as ectopic axonal spikes, but reasonably expected to occur *in vivo*, given the high rates of spontaneous Purkinje cell somatic firing *in vivo* (dozens of Hz; Armstrong & Rawson, 1979; Demer *et al.*, 1985; similar to the rates used in our model); the *in vivo* firing might also be ectopic in origin, at least in part.

The model network oscillation is associated with somatic spikelets (Fig. 2); note that during experimental *in vitro* cerebellar VFO, induced by nicotine + gabazine, spikelets also occur, at least in a subset of Purkinje cells (Middleton *et al.*, 2008). Shape parameters for the great majority of spikelets are continuously and broadly distributed, as in experiments, suggesting that the spikelets result from electrical coupling between different sites of homologous cell regions. The oscillation period is largely determined by the recovery from inactivation of the transient Na^+ current (Figs 7 and 8). The oscillation mechanism can not be understood as a system of coupled single-cell oscillators (each with an intrinsic period similar to the population period), but rather as a more subtle type of cooperativity, in which gap junctions significantly increase the degree of firing (Fig. 4) – although this increase in firing is nowhere near as great as occurs in our models of hippocampal VFO (Traub *et al.*, 1999; see also Lewis & Rinzel, 2000). In the cerebellar VFO model, this latter reduced degree of amplification, produced by electrical coupling, comes about because, in the cerebellar VFO model, a spike in a single axon is not sufficient to induce a spike in a coupled axon.

Omission of cerebellar interneurons

In mouse cerebellar slices, VFO involves cerebellar interneurons as well as Purkinje cells (Middleton, 2005; Middleton *et al.*, 2008) whereas, in our network model, we considered (for the sake of simplicity) only the Purkinje cells. Is this a reasonable assumption? Testing the assumption with experimental electrophysiological methods is not straightforward: one would like to uncouple functionally the putative networks of Purkinje neurons vis-à-vis local circuit interneurons, but there is no simple means to accomplish this. It might be possible to arrange by the transgenic insertion of a protein into the interneurons that selectively allows their hyperpolarization. An additional crucial piece of missing information is morphological (see also below): are there enough gap junctions between Purkinje cells to support the oscillation? Or is it possible that one or more of the interneuron populations is densely interconnected enough by gap junctions to serve as a primary VFO generator that is then transmitted to the Purkinje cells? The latter notion must at least be considered, as there is dye-coupling between Purkinje cells and interneurons (Middleton *et al.*, 2008); on the other hand, experimental *in vitro* VFO power is maximal in the granular layer and white matter (Fig. 7 of Middleton *et al.*, 2008), which might argue against a primary involvement of basket cells and stellate cells. Future simulations of networks containing both Purkinje cells and interneurons, together, may provide clues.

Physical realizability of the proposed gap junctionally connected axonal plexus

In our model, 5 gap junctions (on average) are located all on the proximal 30 μm of each Purkinje cell unmyelinated axon/initial segment. This represents a mathematical idealization, as it is not clear that the Purkinje cells and their axons can be arranged in space in such a way that this is physically realizable: the soma diameter of rat Purkinje cells of postnatal day 18 and above is 17–23 μm (Takács & Hámori, 1994). With the Purkinje somata arranged in a 2D sheet, soma separations would have to be at least 17 μm, and 30 μm of axon does not provide enough length for all the necessary gap junctions, even if each axon is constrained to contact only axons of nearest-neighbor somata (and we assume random axonal electrical connectivity). Therefore, if our model really is capturing the physical principles of cerebellar VFO in a reasonable way, then we must assume either: (i) that some of the gap junctions lie on axon collaterals (we consider this the most likely case); (ii) that axons are coupled on more distal axonal sites than simulated in our model; or (iii) that electrical coupling between Purkinje cells in reality occurs in some indirect fashion, such as through the presynaptic terminals of basket cells. In all of these cases, we would expect the fundamental physical principles of this model to apply, but details are likely to vary – particularly how many axons must discharge together to force the firing in a coupled axon.

Evidence for axonal gap junctions

Dye-coupling between Purkinje cells (Middleton *et al.*, 2008) indicates that Purkinje cells might be electrically coupled, but does not constitute proof for such coupling, let alone that the coupling is between axons. To the best of our knowledge there is only one report that provides ultrastructural evidence (outside of the retina and GABAergic terminals (Muller *et al.*, 2005)) for axonal gap junctions in the mammalian brain, and that report dealt with hippocampal mossy fibers (Hamzei-Sichani *et al.*, 2007). There is, additionally, convincing ultrastructural evidence for gap junctions on the proximal axons of neurons in lower vertebrates (e.g. Korn *et al.*, 1977). We were not able to replicate, in a network model containing only Purkinje cells, the experimental electrophysiological data from cerebellar slices (Middleton, 2005; Middleton *et al.*, 2008) when we used soma-dendritic electrical coupling between the neurons, but we could replicate the data if we postulated electrical coupling between the axons of these cells. In that sense, then, our model makes a precise prediction, namely that such axonal gap junctions do indeed exist. How might they be found? There is considerable evidence that many, or possibly even most, of the gap junctions in the mammalian nervous system are quite small, < 100 nm across (Rash *et al.*, 2007; J. E. Rash, personal communication), as was true for the gap junctions on mossy fibers (Hamzei-Sichani *et al.*, 2007) and, as a consequence, many or most of the gap junctions in the mammalian nervous system will be difficult or impossible to find with conventional thin section transmission electron microscopy. It would appear that freeze-fracture replica immunogold labeling ('FRIL') is the method of choice in order to search for gap junctions (Rash *et al.*, 2007), and we await its application to the cerebellum.

Comparison with a previous study

Maex & De Schutter (2007) were the first, to our knowledge, to address the problem of cerebellar VFO using a network model. Their model had somewhat different structural features and dynamical behaviors than ours, which we may contrast as follows: (i) in the individual neurons, Maex and De Schutter used a very long unmyelinated axon (> 1 mm), whereas we used a short one (tens of μm); (ii) Maex and De Schutter used (mostly) an hexagonal lattice connection topology, while we used a locally random one; (iii) Maex and De Schutter used (mostly) electrical coupling that was located

hundreds of μm from the soma, whereas ours was on the most proximal axon. As a source of stimulation to the neurons, Maex and De Schutter used noisy dendritic synaptic stimulation, whereas we used Poisson-distributed spontaneous axonal spikes.

In terms of dynamics, Maex and De Schutter considered two regimes, weak electrical coupling and strong (with gap junction conductances, in the latter case, able to assume values as large as 9 nS). Here, 'weak coupling' means that single spikes do not cross from axon to axon, whereas with 'large coupling' they do: the dynamical behaviors illustrated in the present paper correspond to 'weak coupling' – indeed, in both studies it was not possible to produce strong coupling with gap junctions located on the proximal axon. For weak coupling, Maex and De Schutter (their fig. 2) found gamma oscillations rather than the VFO described here. Whether the underlying physics of the two models is really identical (neglecting for the moment the issue of frequency) is uncertain, because Maex and De Schutter did not illustrate the firing behaviors of the uncoupled neurons, whereas our Fig. 4 clearly shows that the simulated network oscillation is an emergent phenomenon that can arise from a system of neurons which, when uncoupled, may fire sparsely and irregularly. Our guess, however, is that the Maex and De Schutter model might – if stimulated sufficiently (and perhaps requiring axonal as well as dendritic excitation) – also generate VFO with weak coupling. If this turns out to be true, then the underlying physical mechanisms in the two models could prove similar; such a finding would be interesting, as it would imply that other structural features of the models, such as connection topology, are less relevant.

The VFO that Maex & De Schutter (2007) observed with strong coupling had a number of unusual features, such as: (i) frequency dependence on gap junction site and on the time for an axonal spike to reflect off the soma and conduct back into the axon; and (ii) a tendency of the fastest oscillations to stop and start abruptly. As our model did not possess the corresponding structural features of Maex and De Schutter (very long axon, very strong coupling), we did not observe these corresponding network behaviors. Our guess, however, is that the strong-coupling type of VFO, described by Maex & De Schutter (2007), might be possible if electrical coupling were to occur between Purkinje cell nodes of Ranvier, i.e. at sites distant from the soma. This point again underscores the importance of ultrastructural data for distinguishing oscillation models.

Possible functional significance of cerebellar VFO

In attempting to understand the functional significance of cerebellar VFO, there are several features of the VFO to consider.

1. It is possible that cerebellar VFO in 'pure form', such as occurs *in vitro* with nicotine and gabazine, may exist *in vivo* only as a pathological phenomenon (Cheron *et al.*, 2004, 2005a, b; Servais & Cheron, 2005; Servais *et al.*, 2005); the *in vitro* data suggest that 'pure VFO' *in vivo* might reflect, in part, a failure of local synaptic inhibition (Middleton *et al.*, 2008), as blockade of such inhibition is what converts gamma into VFO. As such, *in vivo* VFO could conceivably contribute to neurological signs such as ataxia; although it is also possible that *in vivo* VFO represents an attempt by the brain to compensate for a functional deficit. In order to address this issue, it would be helpful to have experimental means of manipulating cerebellar VFO in awake behaving mice.
2. Axonal (and somatic) firing during VFO occurs more frequently than would occur without VFO, in conditions where $GABA_A$ receptors are blocked (Fig. 4). Because of the very limited dendritic backpropagation of somatic action potentials in cerebellar Purkinje cells (Llinás & Sugimori, 1980a, b), it seems unlikely that the increased somatic firing would have much influence on synaptic plasticity in Purkinje cell dendrites. On the other hand, the increased orthodromic output from a network of Purkinje cells could have a major effect on downstream neurons, such as neurons in deep cerebellar nuclei. *In vivo* recordings from these latter neurons, during the localized induction of cerebellar VFO, would shed light on this possibility. Does the spatiotemporal patterning – i.e. the fact that VFO really is an oscillation rather than an unstructured increase in axonal firing rates – matter? This issue might be addressable experimentally *in vivo* by comparing the effects of non-specific increases in Purkinje cell excitability with the effects of VFO itself.
3. Complex spikes in Purkinje cells, that result from climbing fiber inputs, represent a form of VFO in single neurons, although at frequencies faster than studied in this paper. Purkinje cells can receive near-simultaneous climbing fiber inputs (Lang *et al.*, 1999), perhaps related to electrical coupling in the inferior olive, the site of origin of the climbing fibers, or to collateralization by the climbing fibers. It is possible that Purkinje axonal coupling would then lead to coordinated VFO in a group of nearby Purkinje neurons – a cerebellar cell assembly, so to speak.

While the above questions remain to be addressed experimentally, one can say at this point that cerebellar VFO is of great interest theoretically because of its different properties as compared with VFO in the hippocampus and neocortex. As noted above, the generation of a similar phenomenon by different means, in distinct brain regions, suggests the possibility of functional relevance.

Supporting information

Additional Supporting Information may be found in the online version of this article:

Fig. S1. Architecture of model Purkinje cell.

Fig. S2. Simulated antidromic and complex spikes in model Purkinje cell.

Fig. S3. Tonic and repetitive burst firing in the model Purkinje cell, in response to a large depolarizing current pulse injected at the soma.

Please note: Wiley-Blackwell are not responsible for the content or functionality of any supporting materials supplied by the authors. Any queries (other than missing material) should be directed to the corresponding author for the article.

Acknowledgements

This study was supported by NIH/NINDS, the Wellcome Trust, MRC and RIKEN. We thank Drs Hiroshi Miyakawa, Walter Akemann and Andrea Bibbig for generous assistance.

Abbreviations

aCSF, artificial cerebrospinal fluid; GABA, γ-aminobutyric acid; VFO, very fast oscillation.

References

Akemann, W. & Knöpfel, T. (2006) Interaction of Kv3 potassium channels and resurgent sodium current influences the rate of spontaneous firing of Purkinje neurons. *J. Neurosci.*, **26**, 4602–4612.

Armstrong, D.M. & Rawson, J.A. (1979) Activity patterns of cerebellar cortical neurones and climbing fibre afferents in the awake cat. *J. Physiol.*, **289**, 425–448.

Cheron, G., Gall, D., Servais, L., Dan, B., Maex, R. & Schiffmann, S.N. (2004) Inactivation of calcium-binding protein genes induces 160 Hz oscillations in the cerebellar cortex of alert mice. *J. Neurosci.*, **24**, 434–441.

Cheron, G., Servais, L., Dan, B., Gall, D., Roussel, C. & Schiffmann, S.N. (2005a) Fast oscillation in the cerebellar cortex of calcium binding protein-deficient mice: a new sensorimotor arrest rhythm. *Prog. Brain Res.*, **148**, 165–180.

Cheron, G., Servais, L., Wagstaff, J. & Dan, B. (2005b) Fast cerebellar oscillation associated with ataxia in a mouse model of Angelman syndrome. *Neuroscience*, **130**, 631–637.

Clark, B.A., Monsivais, P., Branco, T., London, M. & Häusser, M. (2005) The site of action potential initiation in cerebellar Purkinje neurons. *Nat. Neurosci.*, **8**, 137–139.

Coombs, J.S., Curtis, D.R. & Eccles, J.C. (1957) The generation of impulses in motoneurones. *J. Physiol.*, **139**, 232–249.

Courtemanche, R. & Lamarre, Y. (2005) Local field potential oscillations in primate cerebellar cortex: synchronization with cerebral cortex during active and passive expectancy. *J. Neurophysiol.*, **93**, 2039–2052.

Cunningham, M.O., Whittington, M.A., Bibbig, A., Roopun, A., LeBeau, F.E.N., Vogt, A., Monyer, H., Buhl, E.H. & Traub, R.D. (2004a) A role for fast rhythmic bursting neurons in cortical gamma oscillations in vitro. *Proc. Natl Acad. Sci. USA*, **101**, 7152–7157.

Cunningham, M.O., Halliday, D.M., Davies, C.H., Traub, R.D., Buhl, E.H. & Whittington, M.A. (2004b) Coexistence of gamma and high-frequency oscillations in the medial entorhinal cortex *in vitro*. *J. Physiol.*, **559**, 347–353.

De Schutter, E. & Bower, J.M. (1994a) An active membrane model of the cerebellar Purkinje cell I. Simulation of current clamps in slice. *J. Neurophysiol.*, **71**, 375–400.

De Schutter, E. & Bower, J.M. (1994b) An active membrane model of the cerebellar Purkinje cell II. Simulation of synaptic responses. *J. Neurophysiol.*, **71**, 401–419.

Demer, J.L., Echelman, D. & Robinson, D.A. (1985) Effects of electrical stimulation and reversible lesions of the olivocerebellar pathway on Purkinje cell activity in the flocculus of the cat. *Brain Res.*, **346**, 22–31.

Draguhn, A., Traub, R.D., Schmitz, D. & Jefferys, J.G.R. (1998) Electrical coupling underlies high-frequency oscillations in the hippocampus *in vitro*. *Nature*, **394**, 189–192.

Eccles, J.C., Ito, M. & Szentágothai, J. (1967) *The Cerebellum as a Neuronal Machine*. Springer, New York, NY.

Erdös, P. & Rényi, A. (1960) On the evolution of random graphs. *Publ. Math. Inst. Hungar. Acad. Sci.*, **5**, 17–61.

Grieco, T.M. & Raman, I.M. (2004) Production of resurgent current in $Na_v1.6$-null Purkinje neurons by slowing sodium channel inactivation with β-pompilidotoxin. *J. Neurosci.*, **24**, 35–42.

Hamzei-Sichani, F., Kamasawa, N., Janssen, W.G.M., Yasamura, T., Davidson, K.G.V., Hof, P.R., Wearne, S.L., Stewart, M.G., Young, S.R., Whittington, M.A., Rash, J.E. & Traub, R.D. (2007) Gap junctions on hippocampal mossy fiber axons demonstrated by thin-section electron microscopy and freeze-fracture replica immunogold labeling. *Proc. Natl Acad. Sci. USA*, **104**, 12548–12553.

Kato, T. & Hirano, A. (1985) A Golgi study of the proximal portion of the human Purkinje cell axon. *Acta Neuropathol.*, **68**, 191–195.

Kawai, H., Lazar, R. & Metherate, R. (2007) Nicotinic control of axon excitability regulates thalamocortical transmission. *Nat. Neurosci.*, **10**, 1168–1175.

Khaliq, Z.M. & Raman, I.M. (2006) Relative contributions of axonal and somatic Na channels to action potential initiation in cerebellar Purkinje neurons. *J. Neurosci.*, **26**, 1935–1944.

Korn, H., Sotelo, C. & Bennett, M.V.L. (1977) The lateral vestibular nucleus of the toadfish *Opsanus tau*: ultrastructural and electrophysiological observations with special reference to electrotonic transmission. *Neuroscience*, **2**, 851–884.

Lang, E.J., Sugihara, I., Welsh, J.P. & Llinás, R. (1999) Patterns of spontaneous Purkinje cell complex spike activity in the awake rat. *J. Neurosci.*, **19**, 2728–2739.

Lewis, T.J. & Rinzel, J. (2000) Self-organized synchronous oscillations in a network of excitable cells coupled by gap junctions. *Network: Comput. Neural Syst.*, **11**, 299–320.

Llinás, R. & Sugimori, M. (1980a) Electrophysiological properties of *in vitro* Purkinje cell somata in mammalian cerebellar slices. *J. Physiol.*, **305**, 171–195.

Llinás, R. & Sugimori, M. (1980b) Electrophysiological properties of *in vitro* Purkinje cell dendrites in mammalian cerebellar slices. *J. Physiol.*, **305**, 197–213.

Maex, R. & De Schutter, E. (2007) Mechanism of spontaneous and self-sustained oscillations in networks connected through axo-axonal gap junctions. *Eur. J. Neurosci.*, **25**, 3347–3358.

Martina, M., Schultz, J.H., Ehmke, H., Monyer, H. & Jonas, P. (1998) Functional and molecular differences between voltage-gated K^+ channels of fast-spiking interneurons and pyramidal neurons of rat hippocampus. *J. Neurosci.*, **18**, 8111–8125.

Martina, M., Yao, G.L. & Bean, B.P. (2003) Properties and functional role of voltage-dependent potassium channels in dendrites of rat cerebellar Purkinje neurons. *J. Neurosci.*, **23**, 5698–5707.

Middleton, S.J. (2005) *Oscillatory Activity in the Mouse Cerebellum In Vitro*. Ph.D. Thesis, University of Leeds, UK.

Middleton, S.J., Racca, C., Cunningham, M.O., Traub, R.D., Monyer, H., Knöpfel, T., Schofield, I.S., Jenkins, A. & Whittington, M.A. (2008) High frequency network oscillations in cerebellar cortex. *Neuron*, **58**, 1–12.

Miyasho, T., Takagi, H., Suzuki, H., Watanabe, S., Inoue, M., Kudo, Y. & Miyakawa, H. (2001) Low-threshold potassium channels and a low-threshold calcium channel regulate Ca^{2+} spike firing in the dendrites of cerebellar Purkinje neurons: a modeling study. *Brain Res.*, **891**, 106–115.

Muller, J.F., Mascagni, F. & McDonald, A.J. (2005) Coupled networks of parvalbumin-immunoreactive interneurons in the rat basolateral amygdala. *J. Neurosci.*, **25**, 7366–7376.

Nimmrich, V., Maier, N., Schmitz, D. & Draguhn, A. (2005) Induced sharp wave-ripple complexes in the absence of synaptic inhibition in mouse hippocampal slices. *J. Physiol.*, **563**, 663–670.

Pais, I., Hormuzdi, S.G., Monyer, H., Traub, R.D., Wood, I.C., Buhl, E.H., Whittington, M.A. & LeBeau, F.E.N. (2003) Sharp wave-like activity in the hippocampus *in vitro* in mice lacking the gap junction protein connexin 36. *J. Neurophysiol.*, **89**, 2046–2054.

Palay, S.L. & Chan-Palay, V. (1974) *The Cerebellar Cortex*. Springer, New York, NY.

Quian Quiroga, R., Nadasdy, Z. & Ben-Shaul, Y. (2004) Unsupervised spike detection and sorting with wavelets and superparamagnetic clustering. *Neural Comput.*, **16**, 1667–1687.

Rash, J.E., Olson, C.O., Pouliot, W.A., Davidson, K.G., Yasumura, T., Furman, C.S., Royer, S., Kamasawa, N., Nagy, J.I. & Dudek, F.E. (2007) Connexin36 vs. connexin32, "miniature" neuronal gap junctions, and limited electrotonic coupling in rodent suprachiasmatic nucleus. *Neuroscience*, **149**, 350–371.

Roopun, A., Middleton, S.J., Cunningham, M.O., LeBeau, F.E.N., Bibbig, A., Whittington, M.A. & Traub, R.D. (2006) A beta2-frequency (20-30 Hz) oscillation in non-synaptic networks of somatosensory cortex. *Proc. Natl Acad. Sci. USA*, **103**, 15646–15650.

Roth, A. & Häusser, M. (2001) Compartmental models of rat cerebellar Purkinje cells based on simultaneous somatic and dendritic patch-clamp recordings. *J. Physiol.*, **535**, 445–472.

Schmitz, D., Schuchmann, S., Fisahn, A., Draguhn, A., Buhl, E.H., Petrasch-Parwez, R.E., Dermietzel, R., Heinemann, U. & Traub, R.D. (2001) Axo-axonal coupling: a novel mechanism for ultrafast neuronal communication. *Neuron*, **31**, 831–840.

Servais, L. & Cheron, G. (2005) Purkinje cell rhythmicity and synchronicity during modulation of fast cerebellar oscillation. *Neuroscience*, **134**, 1247–1259.

Servais, L., Bearzatto, B., Schwaller, B., Dumont, M., De Saedeleer, C., Dan, B., Barski, J.J., Schiffmann, S.N. & Cheron, G. (2005) Mono- and dual-frequency fast cerebellar oscillation in mice lacking parvalbumin and/or calbindin D-28k. *Eur. J. Neurosci.*, **22**, 861–870.

Servais, L., Hourez, R., Bearzatto, B., Gall, D., Schiffmann, S.N. & Cheron, G. (2007) Purkinje cell dysfunction and alteration of long-term synaptic plasticity in fetal alcohol syndrome. *Proc. Natl Acad. Sci. USA*, **104**, 9858–9863.

Srinivas, M., Rozental, R., Kojima, T., Dermietzel, R., Mehler, M., Condorelli, D.F., Kessler, J.A. & Spray, D.C. (1999) Functional properties of channels formed by the neuronal gap junction protein connexn36. *J. Neurosci.*, **19**, 9848–9855.

Takács, J. & Hámori, J. (1994) Developmental dynamics of Purkinje cells and dendritic spines in rat cerebellar cortex. *J. Neurosci. Res.*, **38**, 515–530.

Traub, R.D., Jefferys, J.G.R., Miles, R., Whittington, M.A. & Tóth, K. (1994) A branching dendritic model of a rodent CA3 pyramidal neurone. *J. Physiol.*, **481**, 79–95.

Traub, R.D., Schmitz, D., Jefferys, J.G.R. & Draguhn, A. (1999) High-frequency population oscillations are predicted to occur in hippocampal

pyramidal neuronal networks interconnected by axoaxonal gap junctions. *Neuroscience*, **92**, 407–426.
Traub, R.D., Draguhn, A., Whittington, M.A., Baldeweg, T., Bibbig, A., Buhl, E.H. & Schmitz, D. (2002) Axonal gap junctions between principal neurons: a novel source of network oscillations, and perhaps epileptogenesis. *Rev. Neurosci.*, **13**, 1–30.
Traub, R.D., Cunningham, M.O., Gloveli, T., LeBeau, F.E.N., Bibbig, A., Buhl, E.H. & Whittington, M.A. (2003a) GABA-enhanced collective behavior in neuronal axons underlies persistent gamma-frequency oscillations. *Proc. Natl Acad. Sci. USA*, **100**, 11047–11052.
Traub, R.D., Pais, I., Bibbig, A., LeBeau, F.E.N., Buhl, E.H., Hormuzdi, S.G., Monyer, H. & Whittington, M.A. (2003b) Contrasting roles of axonal (pyramidal cell) and dendritic (interneuron) electrical coupling in the generation of gamma oscillations in the hippocampus in vitro. *Proc. Natl Acad. Sci. USA*, **100**, 1370–1374.
Traub, R.D., Contreras, D., Cunningham, M.O., Murray, H., LeBeau, F.E.N., Roopun, A., Bibbig, A., Wilent, W.B., Higley, M.J. & Whittington, M.A. (2005) Single-column thalamocortical network model exhibiting gamma oscillations, sleep spindles and epileptogenic bursts. *J. Neurophysiol.*, **93**, 2194–2232.
Yasargil, G.M. & Sandri, C. (1987) Morphology of the Mauthner axon inhibitory system in tench (*Tinca tinca L.*) spinal cord. *Neurosci. Lett.*, **81**, 63–68.

Appendix

Model of single Purkinje cell

We used a highly schematic representation of what might be called an 'average' Purkinje neuron, building on the work of Llinás & Sugimori (1980a, b), Roth & Häusser (2001), De Schutter & Bower (1994a, b), Miyasho *et al.* (2001), and Akemann & Knöpfel (2006). There were 12 voltage- and calcium-dependent conductances: transient Na^+ ($g_{Na(F)}$), persistent Na^+ ($g_{Na(P)}$ – 'P' in this case for 'persistent'), P-type Ca^{2+}($g_{Ca(P)}$ – 'P' here for 'Purkinje'), T-type Ca^{2+}($g_{Ca(T)}$), R-type Ca^{2+}($g_{Ca(R)}$), the anomalous rectifier or '*h*' conductance (g_{AR}), delayed rectifier K^+ ($g_{K(DR)}$), transient inactivating K^+ ($g_{K(A)}$), transient slowly-inactivating K^+ ($g_{K(D)}$), M-type K^+ ($g_{K(M)}$), rapid C-type (BK channel) K^+ that is gated by both voltage and $[Ca^{2+}]_i$ ($g_{K(C)}$), and slow AHP K^+ that is gated by $[Ca^{2+}]_i$ ($g_{K(AHP)}$). Calcium and calcium-gated channels were included for the sake of completeness and for future studies, as they were shut off during the network simulations reported here (as were D channels).
We use a consistent set of units: mV, ms, nF, μS, nA.
The reversal potentials for the various conductances considered are as follows: leak, −80 mV; K^+, −85 mV; Na^+, 45 mV; Ca^{2+}, 135 mV; anomalous rectifier, −30 mV; $GABA_A$, −75 mV; AMPA, 0 mV.

Compartmental architecture and passive parameters

The overall design of the cell is shown in Fig. S1. As in previous publications (e.g. Traub *et al.*, 2005), the model cell was divided into 'levels'; within a given level, each ionic conductance has a fixed density. The definition of the levels is as follows: level 0 is the axon; level 1 is the soma; level 2 is the dendritic shaft; level 3 is the rest of the smooth dendrites; level 4 consists of the spiny dendrites.
All compartments are cylindrical. The radius and length of each compartment was used to compute its internal resistivity; however, the surface area of each spiny dendritic compartment was multiplied by 3 in order to allow for the contribution of the spines. The 'adjusted' surface area was then used for computation of leak conductance and active conductance densities. The soma surface area was 1640 μm^2, the smooth dendritic surface area was 3909 μm^2, and the spiny dendrites (with the spines) were 161 729 μm^2. The radius of the axon tapered linearly from 0.75 to 0.5 μm.
The passive parameters were as follows: internal resistivity, R_i, was 115 Ω−1cm for soma and dendrites, and 100 Ω−1cm for the axon. Membrane resistivity, R_m, was 50 000 Ω−1cm^2 for the dendrites, 10 000 Ω−1cm^2 for the soma and 2000 Ω−1cm^2 for the axon. Membrane capacitance, C_m, was 0.8 μF/cm^2. When all active currents were blocked, the input resistance of the model cell was 35.6 MΩ when measured at the soma, and 79 MΩ when measured in the distal axon.

Discrete form of the cable equation

There are three basic sets of equations to be considered: the cable equation that relates current flows across the membrane and along the interior of the cell; the differential equations for the Hodgkin–Huxley-like state variables that gate the various active conductances; and the equations that govern the internal calcium 'concentration'. The overall approach to these equations is similar to that used in Traub *et al.* (2005).
The discrete form of the cable equation used in a compartmental model has the form (for compartment *k*):

$$C_k \mathrm{d}V_k/\mathrm{d}t = \Sigma_m \gamma_{m,k}(V_m - V_k) - I_{\mathrm{ionic},k}$$

where C_k is the capacitance of the compartment, V_k the transmembrane voltage (and we assume the extracellular space is isopotential), the sum is over compartments *m* that are connected to compartment *k*, $\gamma_{m,k}$ is the conductance (based on internal resistivity) between compartments *m* and *k* (for two coupled cylindrical compartments of equal radius *r* and length *L*, $\gamma_{m,k} = \pi r^2/(R_i L)$ with units chosen appropriately), and $I_{\mathrm{ionic},k}$ consists of the transmembrane ionic currents for the compartment (with the convention that inward current is negative, so that the effect is to make $\mathrm{d}V_k/\mathrm{d}t$ positive, i.e. to depolarize the membrane). $I_{\mathrm{ionic},k}$ has three components: (i) artificially injected currents; (ii) synaptic currents [e.g. something like $g_{GABA(A)}$ ($V_k - V_{GABA(A)}$), where $V_{GABA(A)}$ is the reversal potential]; and (iii) voltage- and calcium-dependent currents. The latter have the general form as follows (for conductance of type 'X'): $g_{k,X(\max)}\, m^\delta h^\varepsilon\, (V_k - V_X)$. Here, $g_{k,X(\max)}$ is the maximal conductance of type *X* in compartment *k* (determined by the area of the compartment, and the conductance density – see tables below); *m* and *h* are Hodgkin–Huxley-like membrane state variables, taking values between 0 and 1: *m* for activation, *h* for inactivation; δ and ε are appropriate integer-valued exponents, with ε = 0 when there is no inactivation; and with *m* and *h* obeying differential equations that depend on membrane voltage and/or calcium concentration; and V_X is the reversal potential for conductance *X*.

Densities of the voltage- and calcium-dependent conductances

Densities of conductances giving rise to (usually, e.g. at resting membrane potential) inward currents (mS/cm^2).

Level	$g_{Na(F)}$	$g_{Na(P)}$	$g_{Ca(P)}$	$g_{Ca(T)}$	$g_{Ca(R)}$	g_{AR}
0	3500	0.1	0.0	0.0	0.0	0.0
1	5000	5.0	0.0	0.0	0.0	0.005
2	10	1.0	0.0	0.5	0.0	0.005
3	0.0	0.0	8.0	1.5	8.0	0.005
4	0.0	0.0	8.0	1.5	8.0	0.005

Densities of conductances giving rise to (usually, e.g. at resting membrane potential) outward currents (mS/cm^2).

Level	$g_{K(DR)}$	$g_{K(A)}$	$g_{K(C)}$	$g_{K(D)}$	$g_{K(M)}$	$g_{K(AHP)}$
0	1000	1.0	0.0	0.0	1.0	0.0
1	1000	15	0.0	0.0	1.0	0.0
2	0.5	80	25	80	1.0	0.0
3	0.5	80	25	80	0.04	1.6
4	0.5	80	25	80	0.04	1.6

Voltage-dependent rate functions (*V* = transmembrane voltage, in mV). α_m (*V*) and β_m (*V*) are the Hodgkin–Huxley forward and backward rate functions, respectively. The state variable *m* obeys the differential equation $\mathrm{d}m/\mathrm{d}t = \alpha_m(V) \times (1 - m) - \beta_m(V) \times m$; *h* obeys an analogous equation. The rate functions are related to the time-constant for relaxation of *m* and to its steady-state value as follows:

$$\tau_m(V) = 1/[\alpha_m(V) + \beta_m(V)];\ m_\infty(V) = \alpha_m(V)/[\alpha_m(V) + \beta_m(V)]$$

We specify the particular form of the various rate functions below, as well as presenting the exponents used for *m* and *h*.
Transient g_{Na}: m^3h (following Miyasho *et al.*, 2001):

$$\alpha_m(V) = 35/\exp(-(V+5)/10)$$

$$\beta_m(V) = 7/\exp((V+65)/20)$$

[Note: these rate functions are shifted 6 mV to the left in the axon, to yield:

$$\alpha_m(V) = 35/\exp(-(V+11)/10), \beta_m(V) = 7/\exp((V+71)/20)]$$

$$\alpha_h(V) = 0.225/(1+\exp((V+80)/10))$$

$$\beta_h(V) = 7.5/\exp(-(V-3)/18)$$

Persistent g_{Na}: m^3 (following Miyasho *et al.*, 2001):

$$\alpha_m(V) = 200/(1+\exp(-(V-18)/16))$$

$$\beta_m(V) = 25/(1+\exp((V+58)/8))$$

P-type g_{Ca}: m (following Miyasho *et al.*, 2001)

$$\alpha_m(V) = 8.5/(1+\exp(-(V-8)/12.5))$$

$$\beta_m(V) = 35/(1+\exp((V+74)/14.5))$$

T-type g_{Ca}: *mh* (following Miyasho *et al.*, 2001)

$$\alpha_m(V) = 2.6/(1+\exp(-(V+21)/8))$$

$$\beta_m(V) = 0.18/(1+\exp((V+40)/4))$$

$$\alpha_h(V) = 0.0025/(1+\exp((V+40)/8))$$

$$\beta_h(V) = 0.19/(1+\exp(-(V+50)/10))$$

R-type g_{Ca}: *mh* (following Miyasho *et al.*, 2001)

$$\alpha_m(V) = 2.6/(1+\exp(-(V+7)/8))$$

$$\beta_m(V) = 0.18/(1+\exp((V+26)/4))$$

$$\alpha_h(V) = 0.0025/(1+\exp((V+32)/8))$$

$$\beta_h(V) = 0.19/(1+\exp(-(V+42)/10))$$

h-current (anomalous rectifier): *m* (Roth & Häusser, 2001)

$$\alpha_m(V) = 0.00063 \times \exp(-0.063H(V+73.2))$$

$$\beta_m(V) = 0.00063 \times \exp(0.079H(V+73.2))$$

Delayed rectifier g_K, *non-inactivating*: m^4 (see Martina *et al.*, 1998, 2003; Traub *et al.*, 2005)

$$m^4(V) = 1/(1+\exp((-V-30)/11.5))$$

$$\text{If } V < -20mV \text{ then } \tau_m(V) = 0.25 + 4.35 \times \exp((V+20)/10);$$

$$\text{otherwise, } \tau_m(V) = 0.25 + 4.35 \times \exp((-V-20)/10)$$

$$\alpha_m(V) = m^4(V)/\tau_m(V)$$

$$\beta_m(V) = 1/\tau_m(V) - \alpha_m(V)$$

M-current: *m*

$$\alpha_m(V) = 0.02/(1.0+\exp((-V-20)/5))$$

$$\beta_m(V) = 0.01 \times \exp((-V-43)/18)$$

A-current: m^4h (Miyasho *et al.*, 2001)

$$\alpha_m(V) = 1.4/(1+\exp(-(V+27)/12))$$

$$\beta_m(V) = 0.49/(1+\exp((V+30)/4))$$

$$\alpha_h(V) = 0.0175/(1+\exp((V+50)/8))$$

$$\beta_h(V) = 1.3/(1+\exp(-(V+13)/10))$$

D-current: m^4h (Miyasho *et al.*, 2001)

$$\alpha_m(V) = 8.5/(1+\exp(-(V+17)/12.5))$$

$$\beta_m(V) = 35/(1+\exp((V+99)/14.5))$$

$$\alpha_h(V) = 0.0015/(1+\exp((V+89)/8))$$

$$\beta_h(V) = 0.0055/(1+\exp(-(V+83)/8))$$

Voltage part of C-current: *m* (kinetics from Traub *et al.*, 1994; with voltage shift of 60 mV, and twofold speed-up)

$$\text{If } V < -10 \text{ mV then}$$

$$\alpha_m(V) = 0.105 \times \exp[(V+50)/11 - (V+53.5)/27]$$

$$\beta_m(V) = 4 \times \exp((-V-53.5)/27) - \alpha_m(V);$$

otherwise

$$\alpha_m(V) = 4H\exp((-V-53.5)/27)$$

$$\beta_m(V) = 0$$

Calcium dynamics and the two calcium-dependent K^+ conductances

The calcium 'concentration' χ (no units) is calculated in each soma-dendritic compartment according to the first-order differential equation

$$d\chi/dt = -\phi I_{Ca} - \beta_\chi \chi$$

here, ψ (in $ms^{-1} \times nA^{-1}$) and β_χ (ms^{-1}) are parameters specific to the compartment, and I_{Ca} is the calcium current for the compartment, in nA (with inward current being negative). ψ = 86 667/(compartment area in μm^2) in the case of a dendritic compartment, and ψ = 173 333/(compartment area in μm^2) for the soma. β_χ = 0.8 for the dendrites, and 0.1 for the soma.

The calcium 'concentration' χ then contributes to the gating of the two calcium-dependent K^+ conductances as follows. For the *C* conductance, in each compartment, $g_{K(C)}$ = [max $g_{K(C)}$ for the compartment] × [Hodgkin–Huxley '*m*' with voltage-dependent kinetics defined above] × Γ; here, Γ = min (1, 0.04 H χ). For the AHP conductance, the Hodgkin–Huxley 'm' variable has kinetics that depend only on χ and not on voltage: α_m (χ) = min (0.0006 × χ, 0.3) and β_m (χ) = 0.06.

Numerical integration

We used our standard second-order explicit method (Traub *et al.*, 2005). The generation of action potentials in this model required a very high density of Na^+ channels in the soma and axon, even with the shift of activation kinetics for Na^+ channels in the axon. As a result, the differential equations are extremely stiff, and a very small integration step (0.6 μs) was required.

Illustrative model behavior

Figures S2 and S3 illustrate examples of the model behavior: antidromic and complex spikes (Fig. S2), and the response to a large depolarizing current (Fig. S3). The latter demonstrates, in particular, the switch between high-frequency repetitive fast spikes and bursts that depend on dendritic calcium spikes.